



A newly developed *qp*-relaxation method for element connectivity parameterization to achieve stress-based topology optimization for geometrically nonlinear structures



Seung Jae Moon, Gil Ho Yoon*

School of Mechanical Engineering, Hanyang University, Seoul, Republic of Korea

ARTICLE INFO

Article history:

Received 22 February 2013

Received in revised form 26 June 2013

Accepted 1 July 2013

Available online 12 July 2013

Keywords:

Stress-based topology optimization

Geometrically nonlinear structure

Element connectivity parameterization method

ABSTRACT

The aim of this work is to present a novel computational approach to employ the stress-based topology optimization method (STOM) to minimize the volume subject to the locally defined stress constraints of a geometrically nonlinear structure in the framework of the element connectivity parameterization (ECP) method. Considering the locally defined stress constraints in topology optimization (TO) is a classic and challenging engineering problem, and successful optimization procedures have recently been developed using the density-based TO method for linear elastic structures. However, no study has yet considered the static failure constraint when using TO for a geometrically nonlinear structure. Therefore, the present study develops a novel computational approach for the STOM for a geometrically nonlinear structure. To successfully optimize a geometrically nonlinear structure, the unstable element issue must be properly addressed, in addition to the stress singularity issue, the existence of a large number of constraints, and the highly nonlinear behavior of the local stress constraints. To effectively resolve these issues, this research adopts the ECP method to interpolate and optimize the connectivities among solid finite elements. Furthermore, we find that a stress singularity issue linked to the local optima issue arises in the ECP method that is different from that of the density-based TO. By investigating the singularity behavior in detail, we develop a new *qp*-relaxation method that is suitable for the ECP method. To demonstrate the improved capability of the proposed ECP method with the modified *qp*-relaxation, several two-dimensional TO problems are solved.

© 2013 Elsevier B.V. All rights reserved.

1. Introduction

This research develops a novel topology optimization (TO) method to address the classic, but still unsolved, challenging TO problem of minimizing a volume subject to local stress constraints, which are defined at the center of every finite element of a geometrically nonlinear structure. Here, it is called the stress-based topology optimization method (STOM) for a geometrically nonlinear structure. Since the introduction of TO in the late 1980s, many studies have focused on applying it to various physics and engineering problems involving linear structural problems, fluid problems, electromagnetic problems, and multiphysics problems [1–9]. In this area of research, one of the most challenging TO problems continues to be minimizing a volume subject to local stress constraints, to prevent static or dynamic failures [1,10–20]. Many studies have demonstrated that numerous theoretical and practical issues remain to be resolved for the rigorous consideration of local stress constraints in TO, including the singular behavior of stress with respect to the density design variables of TO, the highly non-

linear behavior of local stress constraints, and the trade-off between local and global stress constraints [10–13,15–17,19–23]. In addition to these complex issues, from an engineering point of view, the unstable element issue, i.e., the flipped element and negative area element, which are often observed at finite elements with low stiffness values, should be properly addressed for TO problems involving geometrically nonlinear structures [24–28]. To the best of our knowledge, there has been little relevant research related to the STOM problem for geometrically nonlinear structures before the present study. To rigorously study the STOM without the unstable element issue, this research applies the element connectivity parameterization (ECP) method to parameterize the connectivities among solid finite elements, as shown in Fig. 1 [27–30], building on the innovative approaches and important conclusions of the previous relevant research on stress constraint problems [10–13,15–17,19–23].

1.1. Introduction of ECP

Compared with the density-based TO method, topological evolutions in the design domain are differently modeled and represented in the ECP method, as shown in Fig. 1 [27–30]. The

* Corresponding author. Tel.: +82 2 2220 0451.

E-mail addresses: gilho.yoon@gmail.com, ghy@hanyang.ac.kr (G.H. Yoon).

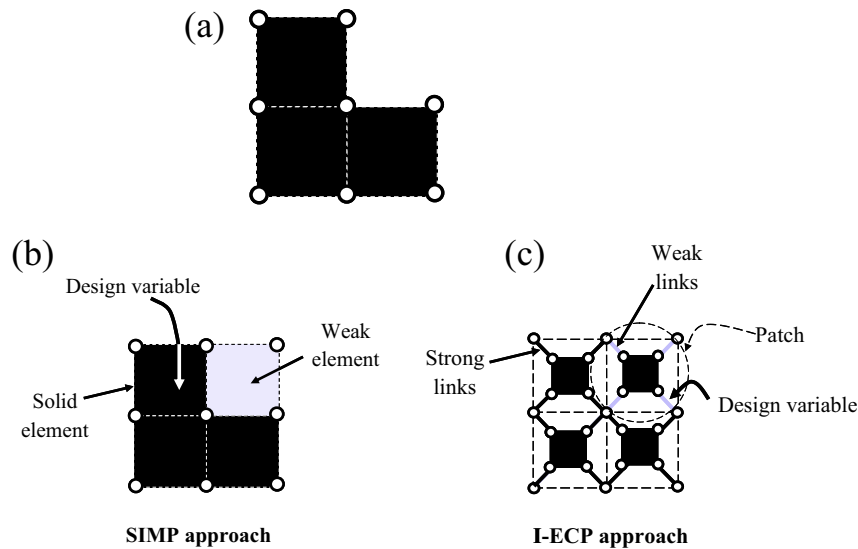


Fig. 1. Comparison of modeling approaches of solid isotropic material with penalization (SIMP) approach and internal ECP method.

allowance of topological changes in the design domain is one of the most important benefits of TO compared with other structural methods that optimize size and shape [1]. This capability makes it possible to obtain new topological connectivities without a given initial design or layout. In the element density-based TO method, a design domain is usually discretized using finite elements. In addition, the elements' material properties are interpolated, such as Young's modulus, thermal conductivity, and electric conductivity, depending on the physics of interest, with respect to the density design variables of the SIMP method or with respect to the microstructure design variables of the homogenization method [1], as shown in Fig. 1(b). By changing the material properties of the finite elements for either void or solid domains, topological modifications can be simulated without alterations of the manifold geometry of an FE model. By finding the design variable values determining the material properties that minimize an objective subject to several constraints, the density-based TO method can provide innovative layouts for engineers. However, assigning a lower-bound design variable value for void or null regions is a shortcoming. For example, there is the critical complication of an unstable element when applying the density-based TO method to a geometrically nonlinear structure whose stress and strain measures are the 2nd Piola–Kirchhoff (PK) stress and the Green–Lagrangian strain, with the Newton–Raphson method as a solution method. Because larger displacements are allowed, unstable elements having negative areas mostly at void regions are inevitably observed. These flipped elements appear only in computer simulations and cannot exist in reality [24,25,28–31]. For these flipped elements with non-positive areas, the tangent stiffness matrix assembled with their stiffness matrices often becomes a non-positive definite. Consequently, stable convergence of the Newton–Raphson iteration cannot be guaranteed with unstable elements. To handle this complex issue, several numerical techniques and various optimization methods have been proposed in the framework of the density-based approach [24,25,28–30]. Among the most recent contributions, a new interpolation method called the ECP method was proposed, as shown in Fig. 1(c) (please see [30] for a MATLAB implementation, along with the Appendix of this paper). In the ECP method, the material properties of the finite elements are not interpolated, but their connections are interpolated, as shown in Fig. 1(c). To account for the topological

changes in the ECP method, zero-length links are used to connect the nodes of the discretized finite elements. Depending on the composition approaches used for the zero-length links and solid elements, the external ECP method and the internal ECP method have been proposed [32]. In the internal ECP method, the static condensation technique for the degrees of freedom of the internal nodes composed of solid elements (discretized finite elements) is applied to reduce the computation time. In short, because the ECP method can effectively handle unstable elements, this research adopts the internal ECP method when applying the STOM to a geometrically nonlinear structure.

1.2. Three inherited issues with STOM

For the successful implementation of the STOM, many theoretical issues should be addressed. First, the singularity issue of the stresses defined at each finite element should be resolved [12,15,20]. The singularity issue involves removing the stress constraints of finite elements simulating a void from an optimization problem. It should be noted that this issue is a separate one, and is not related to the stress singularities due to geometric kinks (discontinuities), concentrated loads, or boundary conditions. (Please see [10] and the reference therein for an introduction.) When the density design variables of the SIMP method for topology optimization reach a lower bound during a simulation of the material properties of void regions, the corresponding finite elements can undergo excessive distortions, even in a linear structure, and the local stress constraint should be removed from the optimization formulation (the so-called vanishing constraint [10,12,13]). Moreover, an optimization algorithm cannot find a local or global optimum with a void and solid without the appearance of grey elements, because the global optimum is located in the degenerated parts of the feasible domain (see the three-bar truss design in [12] and Refs. [10,13]). To solve this singularity issue, many relaxation methods have been proposed, such as the epsilon-relaxation method [12], the qp -relaxation method [10,11,22,33], and the relaxed stress indicator [34]. In this research, the qp -relaxation method is employed.

Second, the stress constraints defined at every finite element should be carefully managed by an efficient optimization solver [34–36]. In other words, it is almost impossible to solve an optimization problem with refined element-wise stress constraints within a

moderate computation time. From an optimization point of view, this issue is closely related to the development of an efficient dual optimizer. Some global constraint approaches have been developed merely to ensure that the maximum stress value is less than a prescribed limit. Additionally, several numerical approaches have been proposed for global constraint approaches, such as the aggregation function [18,23], p -norm [1], and segregated global stress norms [15,17,23]. Third, the highly nonlinear behavior of the stress constraints should be addressed [13,15]. To accomplish this, an accurate and efficient gradient-based optimizer should be employed.

1.3. Singularity issue of ECP method

In addition to the above issues, the stress interpolation issue for the ECP method and the serious stress singularity issue (vanishing stress constraint) of the 2nd PK stress should be addressed when using the STOM for a geometrically nonlinear structure. The stress singularity issues of the 2nd PK and Cauchy stress are similar, as discussed in the analysis examples in Section 4. As shown in Fig. 1, the material properties of the discretizing finite elements remain constant and are not altered in the ECP method for the forward analysis. However, it is found that, when conducting the sensitivity analysis, it is necessary to interpolate the constitutive matrices of the discretizing elements with respect to the design variables determining the stiffness values of the zero-length link. Without the additional interpolation of the constitutive matrices as an alternative formulation to the qp -relaxation, the stress singularity issue remains, and non-structure (local optima) becomes an optimum design, even in the ECP method. To cope with this stress singularity issue and the local optima issue of the ECP method, a special interpolation scheme for the constitutive matrix is devised in this research by investigating the stress behavior of the qp -relaxation of the density-based topology optimization. In addition, the 2nd PK stress increases in the ECP method when the quadratic term is added for the Green–Lagrangian strain. In short, this paper presents a modified qp -relaxation technique for the singularity issue and the local optima issue of the ECP method.

1.4. New qp -relaxation technique for ECP method

A new version of the qp -relaxation method is required when using the STOM for a geometrical nonlinear structure. Among the many available relaxation methods, the qp -relaxation method, in which different penalization factors are employed for the forward and sensitivity analyses, has been widely and successfully used for the TO of linear structures (see [1,10,12] and the references therein). In the qp -relaxation method, by employing different penalty values for the constitutive matrices for the analyses in the SIMP method, it seems that void regions having weak stiffness values and experiencing excessive distortions with non-zero stress values are discouraged from an optimization point of view; this will be investigated in the section discussing numerical approaches. The ECP method does not interpolate the material properties of the finite elements with respect to the design variables; rather, it parameterizes the connectivities among the solid finite elements. Therefore, from the viewpoint of the SIMP method, the penalization factor of the design variable of the discretizing elements can be regarded as set to 0. This research shows that, although the discretizing elements remain constant, the stress singularity issue and local optima issue become problematic for the ECP method. Although the ECP method does not interpolate the material properties in the forward analysis, we should interpolate the constitutive matrix in the sensitivity analysis process with respect to the design variables to obtain physically acceptable layouts. An improper choice for

the stress penalization exponent of the qp -approach can lead to solutions with numerous grey elements (please see [10] for suggestions of qp values to overcome the gray region issue and [13] for an interesting discussion). In addition, by solving an elementary beam structure with different combinations of penalty factors in the example section, we show that the qp -relaxation method of the density-based approach also plays a partial role as a regulation method that helps prevent the stress-based topology optimization from having “no-structure.” We agree that it cannot be generalized in complex problems with different boundary conditions. Indeed, no-structure with stress values of zero minimizes the volume, as well as satisfies the local stress constraints at all finite elements. From an optimization point of view, no-structure also becomes a global optimum solution. It is worthwhile to emphasize once again that the features of the ECP method include the fact that it does not require interpolation of the material properties for forward analysis, and it shows some advantages for a nonlinear structure. Thus, this paper shows that the ECP method also requires some material interpolation satisfying a special condition in the sensitivity analysis for the STOM, which minimizes the volume subject to local stress constraints. Finally, this research investigates the stress behavior of the density-based approach and proposes a new qp -relaxation technique suitable for the ECP method that regularizes the optimization process by making no-structure an unfavorable solution.

The rest of this paper is organized as follows. First, we present stress-based topology optimization formulations based on the SIMP method and the ECP method, along with sensitivity analyses of the aggregated global stress constraints, which were developed to resolve the issue of one global stress constraint. In addition, some issues that arise when implementing the STOM are explained in Section 2. In Section 3, we describe the development of the novel procedure for the ECP method to resolve the multiple issues that have been raised. In the numerical example section, to show the validity and versatility of the present approach, we provide simple structure analyses and some two-dimensional topology optimization problems. Finally, the conclusions and observations of this research are given in the conclusions section.

2. Stress analysis of geometrically nonlinear structure using internal ECP method

2.1. Stress analysis of geometrically nonlinear structure

The situation of large structural displacements due to large structural forces in an elastic or nonlinear homogeneous medium can be treated with the standard Galerkin approximation of weak forms [37,38]. Rather than using the linear elastic strain and stress measures, we employ the Green–Lagrangian strain by adding the appropriate quadratic term to the linear strain measure and the associated 2nd PK stress, as follows:

$${}^{t+\Delta t}_0 \mathbf{c}_{ij} = \frac{1}{2} \left({}^{t+\Delta t}_0 \mathbf{u}_{i,j} + {}^{t+\Delta t}_0 \mathbf{u}_{j,i} + {}^{t+\Delta t}_0 \mathbf{u}_{i,i} {}^{t+\Delta t}_0 \mathbf{u}_{j,j} \right) \quad (i = 1, 2 \text{ for 2D and } 1, 2, 3 \text{ for 3D}) \quad (1)$$

$$\frac{\partial {}^{t+\Delta t}_0 S_{ij}}{\partial {}^{t+\Delta t}_0 \epsilon_{rs}} = {}^0 c_{ijrs} \quad (i = 1, 2 \text{ for 2D and } 1, 2, 3 \text{ for 3D}) \quad (2)$$

$$\mathbf{S} = \mathbf{CE} \quad (3)$$

where the displacement component in the x_i coordinate at time $t + \Delta t$ is ${}^{t+\Delta t}_0 u_i$. The left subscript 0 is used to indicate that the corresponding displacements and strains are measured for the non-deformed configuration. The comma in the displacements denotes

partial differentiation with respect to the coordinate. The vector expressions of the second PK stress and Green–Lagrangian strain are given by \mathbf{S} and \mathbf{E} , respectively, and they are assumed to be related through a linear constitutive matrix \mathbf{C} (the Kirchhoff material assumption) [37,38].

It is common to denote the displacement increment nodal vector as $\Delta\mathbf{U}$ and the displacement nodal vector at time $t + \Delta t$ as ${}^{t+\Delta t}\mathbf{U}$, for a generic point of a body at domain V in equilibrium. Then, the following update rules for the Newton–Raphson method can be used (see [37–39]):

$$\mathfrak{R} = {}^{t+\Delta t}\mathbf{F}_{\text{Ext}} - {}^{t+\Delta t}\mathbf{F}_{\text{Int}} = {}^{t+\Delta t}\mathbf{F}_{\text{Ext}} - \int_{V_0} \mathbf{B}_{nl}^T \mathbf{S} dV_0 = \mathbf{0} \quad (4)$$

$${}^t\mathbf{K}_T = \frac{\partial \mathfrak{R}}{\partial {}^{t+\Delta t}\mathbf{U}} \quad (5)$$

$${}^{t+\Delta t}\mathbf{U}^{(k)} = {}^{t+\Delta t}\mathbf{U}^{(k-1)} + \Delta\mathbf{U}^{(k)}, \quad {}^{t+\Delta t}\mathbf{U}^{(0)} = {}^t\mathbf{U} \quad (6)$$

$${}^t\mathbf{K}_T^{(k-1)} \Delta\mathbf{U}^{(k)} = \mathfrak{R}({}^{t+\Delta t}\mathbf{U}^{(k-1)}) \quad (7)$$

where the superscript k denotes the iteration step in the implemented Newton–Raphson method. The residual vector and tangent stiffness matrix are denoted by \mathfrak{R} and ${}^t\mathbf{K}_T$, respectively. The nonlinear strain–displacement matrix is denoted by \mathbf{B}_{nl} [38]. The symbols ${}^{t+\Delta t}\mathbf{F}_{\text{Ext}}$ and ${}^{t+\Delta t}\mathbf{F}_{\text{Int}}$ denote the external load and internal load, respectively.

2.2. Nonlinear static analysis using ECP method

Unlike the density-based approach that defines topological changes by interpolating material properties, the ECP method chooses an alternative strategy to define topological changes, as shown in Fig. 1. Compared with the element density-based TO method, the ECP method has a unique feature where plane or cubic finite elements, called discretizing elements, remain solid. The disconnected finite elements are joined using one-dimensional zero-length links, and the group consisting of a discretizing element, links, and nodes defining zero-length links is called a *patch*. In a patch, the nodes used to construct discretizing elements are called inner nodes, whereas the nodes connecting the outer nodes of different discretizing finite elements are called outer nodes. Because of the newly introduced nodes and the separated nodes with the same spatial locations, the number of degrees of freedom of the ECP method is much higher than the number of degrees of freedom of the density-based method, which inevitably increases the computation time. To reduce the computation time, the static condensation scheme should be applied to the patch [30,32].

Initially, the displacements of the outer nodes and inner nodes for the k th iteration are denoted as ${}^{t+\Delta t}\mathbf{u}_{e,\text{out}}^{(k)}$ and ${}^{t+\Delta t}\mathbf{u}_{e,\text{in}}^{(k)}$, respectively. These displacements are updated in the Newton–Raphson method, as follows:

$$\begin{bmatrix} {}^{t+\Delta t}\mathbf{u}_{e,\text{out}}^{(k)} \\ {}^{t+\Delta t}\mathbf{u}_{e,\text{in}}^{(k)} \end{bmatrix} = \begin{bmatrix} {}^{t+\Delta t}\mathbf{u}_{e,\text{out}}^{(k-1)} \\ {}^{t+\Delta t}\mathbf{u}_{e,\text{in}}^{(k-1)} \end{bmatrix} + \begin{bmatrix} \Delta\mathbf{u}_{e,\text{out}}^{(k)} \\ \Delta\mathbf{u}_{e,\text{in}}^{(k)} \end{bmatrix} \quad (8)$$

where $\Delta\mathbf{u}_{e,\text{out}}^{(k)}$ and $\Delta\mathbf{u}_{e,\text{in}}^{(k)}$ are the updated displacements for the outer nodes and inner nodes, respectively. The incremental displacements of the outer and inner nodes are calculated using the following equations:

$$\mathbf{k}_{l,e} = l_e(\gamma_e) \mathbf{I}_{8 \times 8}, \quad \text{where } \mathbf{I}_{8 \times 8} \text{ is an } 8 \times 8 \text{ identity matrix} \quad (9)$$

$$\left\{ \begin{bmatrix} \mathbf{k}_{l,e} & -\mathbf{k}_{l,e} \\ -\mathbf{k}_{l,e} & \mathbf{k}_{l,e} \end{bmatrix} + \begin{bmatrix} \mathbf{0} & \mathbf{0} \\ \mathbf{0} & {}^t\mathbf{k}_{T,e}^{structure,(k-1)} \end{bmatrix} \right\} \begin{bmatrix} \Delta\mathbf{u}_{e,\text{out}}^{(k)} \\ \Delta\mathbf{u}_{e,\text{in}}^{(k)} \end{bmatrix} = \begin{bmatrix} \mathfrak{R}_{e,\text{out}}^{(k-1)} \\ \mathfrak{R}_{e,\text{in}}^{(k-1)} \end{bmatrix} \quad (10)$$

$$\begin{bmatrix} \mathfrak{R}_{e,\text{out}}^{(k-1)} \\ \mathfrak{R}_{e,\text{in}}^{(k-1)} \end{bmatrix} = \begin{bmatrix} {}^{t+\Delta t}\mathbf{R}_e \\ \mathbf{0} \end{bmatrix} - \begin{bmatrix} \mathbf{0} \\ {}^{t+\Delta t}\mathbf{f}_e^{structure,(k-1)} \end{bmatrix} - \begin{bmatrix} {}^{t+\Delta t}\mathbf{f}_{e,\text{out}}^{link,(k-1)} \\ {}^{t+\Delta t}\mathbf{f}_{e,\text{in}}^{link,(k-1)} \end{bmatrix} \quad (11)$$

$$\begin{bmatrix} {}^{t+\Delta t}\mathbf{f}_{e,\text{out}}^{link,(k-1)} \\ {}^{t+\Delta t}\mathbf{f}_{e,\text{in}}^{link,(k-1)} \end{bmatrix} = \begin{bmatrix} \mathbf{k}_{l,e} & -\mathbf{k}_{l,e} \\ -\mathbf{k}_{l,e} & \mathbf{k}_{l,e} \end{bmatrix} \begin{bmatrix} {}^{t+\Delta t}\mathbf{u}_{e,\text{out}}^{(k-1)} \\ {}^{t+\Delta t}\mathbf{u}_{e,\text{in}}^{(k-1)} \end{bmatrix} \quad (12)$$

$$l_e = \alpha \frac{\gamma_e^{n_{\text{inter}}}}{1 + (1 - \gamma_e^{n_{\text{inter}}})\tau} + \beta \quad \left(\tau = \frac{\alpha \times s}{k_{\text{diagonal}}^{structure} \times k} \right) \quad (13)$$

$$\alpha = l_{\text{max}} - l_{\text{min}}, \quad \beta = l_{\text{min}} \quad (14)$$

$$0 \leq \gamma_e \leq 1, \quad (15)$$

The link stiffness value l_e is a function of the design variable γ_e assigned to the e th patch. The stiffness matrix and residual force terms of the outer and inner nodes of the e th patch are ${}^t\mathbf{k}_{T,e}^{structure,(k-1)}$, $\mathfrak{R}_{e,\text{out}}^{(k-1)}$, and $\mathfrak{R}_{e,\text{in}}^{(k-1)}$, respectively. The external force on the outer nodes and the internal force acting on the inner nodes are ${}^{t+\Delta t}\mathbf{R}_e$ and ${}^{t+\Delta t}\mathbf{f}_e^{structure,(k-1)}$, respectively. The upper and lower stiffness bounds of the links are l_{max} and l_{min} , respectively. For stable optimizations, $n_{\text{inter}} = 3$, $k = 2$, and $s = 10$ are used for the nonlinear analysis, unless otherwise stated.

As discussed, to shorten the computation time, the static condensation scheme is applied as follows:

$${}^t\mathbf{k}_{\text{Con},e}^{(k-1)} = \left(\mathbf{k}_{l,e} - \mathbf{k}_{l,e} \left(\mathbf{k}_{l,e} + {}^{t+\Delta t}\mathbf{k}_{T,e}^{structure,(k-1)} \right)^{-1} \mathbf{k}_{l,e} \right) \quad (16)$$

$${}^t\mathbf{k}_{\text{Con},e}^{(k-1)} \Delta\mathbf{u}_{e,\text{out}}^{(k)} = \mathfrak{R}_{e,\text{out}}^{(k-1)} + \mathbf{k}_{l,e} \left(\mathbf{k}_{l,e} + {}^t\mathbf{k}_{T,e}^{structure,(k-1)} \right)^{-1} \mathfrak{R}_{e,\text{in}}^{(k-1)} \quad (17)$$

Rather than inverting a large stiffness matrix, the global tangent matrix is assembled with the above condensed patch stiffness matrix, as follows:

$${}^t\mathbf{K}_{\text{Con}}^{(k-1)} = \sum_{e=1}^{N_p} {}^t\mathbf{k}_{\text{Con},e}^{(k-1)} \quad (18)$$

Here, the total number of patches is N_p . The standard Newton–Raphson iterations are applied for $\Delta\mathbf{U}_{\text{out}}^{(k)}$, which is the global displacement vector for the outer nodes:

$${}^t\mathbf{K}_{\text{Con}}^{(k-1)} \Delta\mathbf{U}_{\text{out}}^{(k)} = \mathfrak{R}_{\text{Con}}^{(k-1)} \quad (19)$$

$$\text{where } \mathfrak{R}_{\text{Con}}^{(k-1)} = \sum_{e=1}^{N_p} \left[\mathfrak{R}_{e,\text{out}}^{(k-1)} + \mathbf{k}_{l,e} \left(\mathbf{k}_{l,e} + {}^t\mathbf{k}_{T,e}^{structure,(k-1)} \right)^{-1} \mathfrak{R}_{e,\text{in}}^{(k-1)} \right] \quad (20)$$

For NR convergence, we use the following criterion:

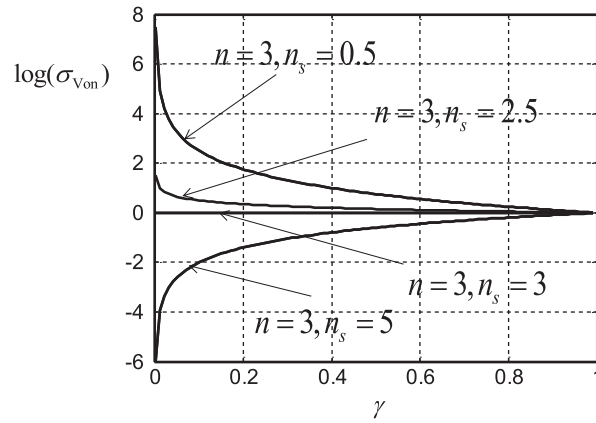
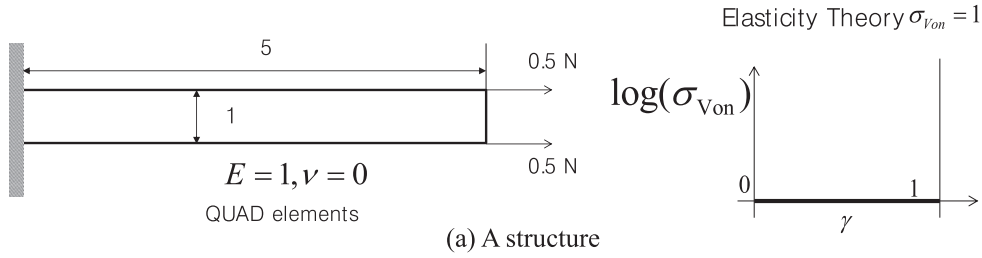
$$\left| \Delta\mathbf{U}_{\text{out}}^{(k)} \right| = \sqrt{\sum_{e=1}^{N_p} \left(\Delta\mathbf{u}_{e,\text{out}}^{(k)} \right)^2} \leq NR_{\text{limit}} \quad (NR_{\text{limit}} = 10^{-11}) \quad (21)$$

After obtaining the converged displacements of Eq. (19) for the degrees of freedom of the outer nodes, the degrees of freedom of the inner nodes are calculated, and the stress components of the discretizing finite elements are evaluated at the center of the finite elements. In the next section, the STOM formulation and sensitivity analysis for a geometrically nonlinear structure are derived and discussed.

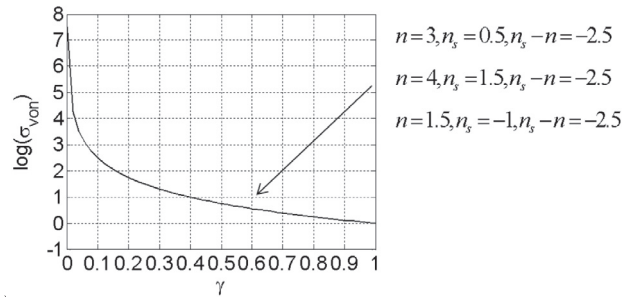
3. Stress-based topology optimization formulation and analytical sensitivity analysis

In this section, brief explanations of the STOM formulation and sensitivity analysis are given [15,20]. Specifically, the penal-

ization method—or the qp -relaxation formulation that defines different penalization factors for the constitutive matrices used for a forward analysis of the structural displacements—and the sensitivity analysis are investigated for the STOM based on the ECP method. In addition, the sensitivity analysis of the

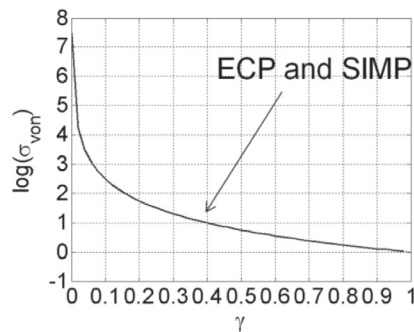


(b) Stress values of element density-based approach



(c) Stress values of element density-based approach

$$n_{ECP_S} = \underbrace{n_s - n}_{SIMP} = 0.5 - 3 = -2.5$$



(d) Stress values of element connectivity parameterization method

Fig. 2. Simple straight structure and stress analyses with various penalty factors. ($l_{\max} = 10^6 \times k_{\text{structure}}^{\text{diagonal}}$, $l_{\min} = 10^{-6} \times k_{\text{structure}}^{\text{diagonal}}$, $l_e = \alpha \frac{\gamma_e^p}{1 + (1 - \gamma_e^p)\tau} + \beta$, $\tau = \frac{l_{\max} \times s}{k_{\text{structure}}^{\text{diagonal}} \times k}$, $s = 1$, $k = 2$).

STOM of the ECP method with the geometric nonlinearity is newly derived.

3.1. Stress-based topology optimization formulation

3.1.1. Optimization formulation

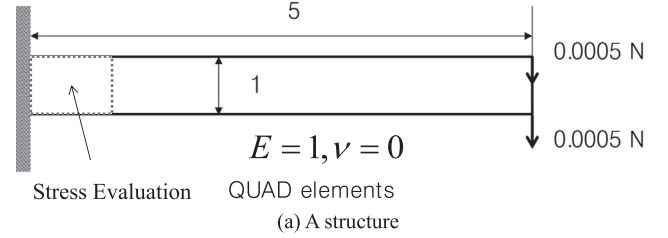
This subsection is devoted to describing the topology optimization formulation considering von Mises stress constraints defined at each finite element. First, to deal with the existence of too many local constraints defined at every finite element, a regional scheme based on the sorting algorithm proposed in [14–17,23] and the p -norm approximation of (24) are also employed for the ECP method, as follows:

$$\begin{aligned}
 & \text{Minimize}_{\gamma} \quad V(\gamma) = \sum_{e=1}^{NE} \tilde{\gamma}_e v_e(\gamma : \text{Filtered density}) \\
 & \text{subject to} \quad \langle \sigma_{\max} \rangle_1 \leq \sigma^* \\
 & \quad \quad \quad \langle \sigma_{\max} \rangle_2 \leq \sigma^* \\
 & \quad \quad \quad \vdots \\
 & \quad \quad \quad \langle \sigma_{\max} \rangle_{RN} \leq \sigma^* \\
 & \quad \quad \quad \tilde{\gamma} = \Xi(\gamma) \text{ with the density filter } \Xi \\
 & \quad \quad \quad \tilde{\gamma}_i = \sum_{j \in \Omega_i} w_j \gamma_j / \sum_{j \in \Omega_i} w_j, w_j = \max(1 - r_{\min}/r_j, 0), r_{\min} : \\
 & \quad \quad \quad \text{filter radius} \\
 & \quad \quad \quad \Omega_i : \text{the neighbor elements of the } i\text{th elements} \\
 & \quad \quad \quad r_j : \text{the distance between the element } i \text{ and } j \text{ centroids}
 \end{aligned} \tag{22}$$

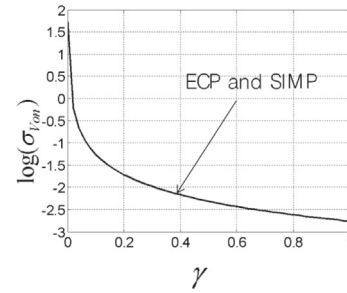
$$\langle \sigma_{\max} \rangle_k^{iter} \equiv c_k^{iter} \langle \sigma_{PN} \rangle_k^{iter} \tag{23}$$

$$\langle \sigma_{PN} \rangle_k^{iter} \equiv \left(\sum_e \left(\frac{\sigma_e}{\sigma^*} \right)^p \gamma_e \right)^{1/p} \quad (e \in \Omega_k) \tag{24}$$

$$c_k^{iter} = \alpha \frac{\sigma_{\max}^{kiter-1}/\sigma^*}{\langle \sigma_{PN} \rangle_k^{iter-1}} + (1 - \alpha) c_k^{iter-1} \tag{25}$$



$$n_{ECP-S} = n_S - n = 0.5 - 3 = -2.5$$



(b) Stress values of element connectivity parameterization method

Fig. 3. Simple straight structure with vertical load.

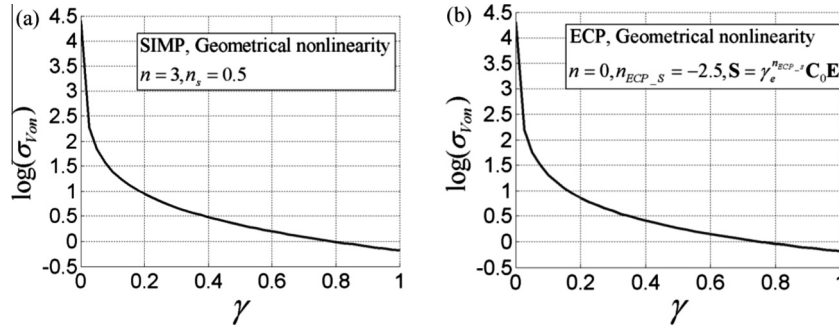


Fig. 4. (a) SIMP and ECP approaches for straight beam of geometrically nonlinear structure for extension load and (b) von Mises stress of 2nd PK stress. (The design variables of the ECP method are set to one.)

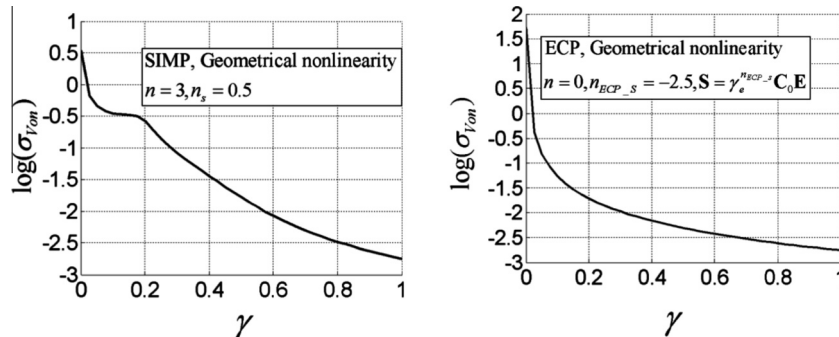


Fig. 5. (a) SIMP and ECP approaches for straight beam of geometrically nonlinear structure for bending load and (b) von Mises stress of 2nd PK stress. (The design variables of the ECP method are set to one.)

$$\sigma_e = \frac{1}{\sqrt{2}} \left[\left(\begin{matrix} t+\Delta t \\ 0 \end{matrix} S_x - \begin{matrix} t+\Delta t \\ 0 \end{matrix} S_y \right)^2 + \left(\begin{matrix} t+\Delta t \\ 0 \end{matrix} S_y - \begin{matrix} t+\Delta t \\ 0 \end{matrix} S_z \right)^2 + \right. \\ \left. \left(\begin{matrix} t+\Delta t \\ 0 \end{matrix} S_z - \begin{matrix} t+\Delta t \\ 0 \end{matrix} S_x \right)^2 + 6 \left(\begin{matrix} t+\Delta t \\ 0 \end{matrix} S_{xy}^2 + \begin{matrix} t+\Delta t \\ 0 \end{matrix} S_{yz}^2 + \begin{matrix} t+\Delta t \\ 0 \end{matrix} S_{xz}^2 \right) \right]^{1/2} \quad (26)$$

where the volume of the e th finite element is v_e . Conventional notations are used to indicate the nominal and shear stress components of the finite element in the above formulation. Here, the design variables assigned to the N_p elements of the design domain are denoted as γ and used to interpolate the link stiffness values. It is worth noting that the design variables or the sensitivity values can be filtered as in the SIMP approach [40–44]. To cope with the existence of a large number of constraints, the locally defined stress constraints are aggregated using the regional stress constraints $\langle \sigma_{\max} \rangle_k$ with the stress p -norm of the k th region $\langle \sigma_{PN} \rangle_k^{iter}$. Because there are discrepancies between the p -norm value and the real maximum value, the correction factor c_k^{iter} is introduced, which is the ratio between the stress p -norm and the real maximum stress value $\sigma_{\max,k}^{iter-1}$ in the previous $iter-1$ optimization iteration at the k th region. Here, we should emphasize that the above updating of the correction factor, c_k^{iter} , is heuristic. In other words, the index order of the finite elements for each region is subject to change during an optimization,

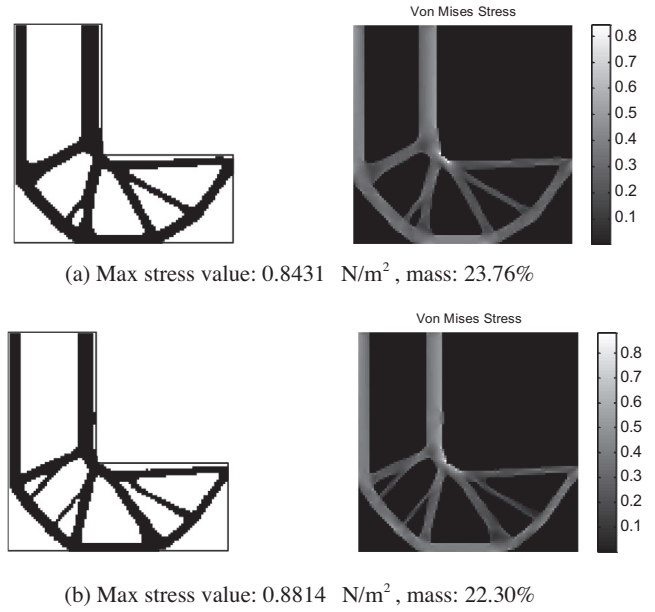
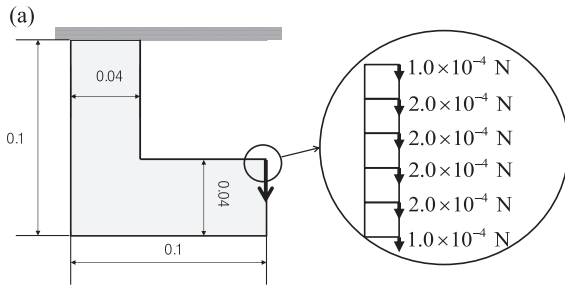
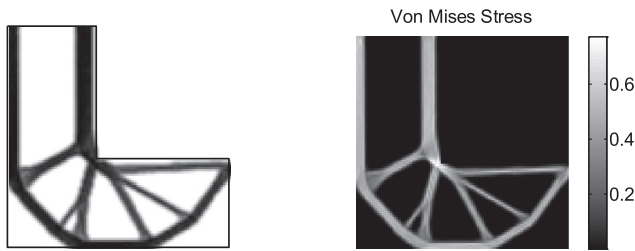


Fig. 7. Postprocessing of L-shaped structure of Fig. 6 (hard-kill criterion: 0.35).

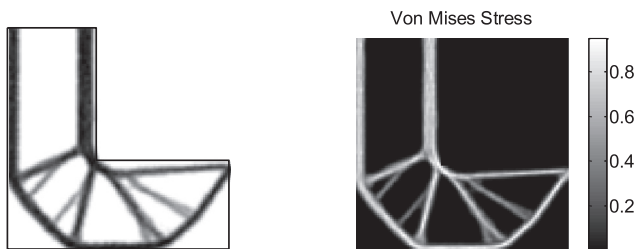


$E = 10^6 \text{ N/m}^2, \nu = 0.3$

100 by 100 QUAD elements



(b) $\sigma^* = 0.8 \text{ N/m}^2$, mass: 20.92%



(c) $\sigma^* = 1 \text{ N/m}^2$, mass: 16.27%

Fig. 6. L-shaped structure and optimization results. (a) A problem definition ($RN = 8$, $n_{\text{inter}} = 3$, $l_{\text{max}}/k_{\text{diagonal}}^{\text{structure}} = 10^9$, $l_{\text{min}}/k_{\text{diagonal}}^{\text{structure}} = 10^{-9}$, radius of filter: 2 times the finite element), (b) an optimized design with 20.92% mass usage for the maximum stress limit $\sigma^* = 0.8 \text{ N/m}^2$, and (c) an optimized design with 16.27% mass usage for the maximum stress limit $\sigma^* = 1 \text{ N/m}^2$.

and the contributing elements for each region are also different; that is, the optimization has a non-differentiable condition. However, in most cases, as the optimization converges, the index order for each region becomes almost stable and fixed. In the case of a geometrical nonlinear analysis, this non-differentiable condition can cause a significant deterioration of the optimization history. Thus, we update the correction factor every few iterations, e.g., at the 10th iteration. The maximum allowable von Mises stress value, σ^* , is provided by engineers to constrain the e th stress value, σ_e .

3.1.2. qp-Relaxation methods of SIMP method and ECP method

From the many relevant studies, it is known that, for stable convergence in the element density method, the constitutive matrices for the static and sensitivity analyses of stress constraints are formulated differently, as follows:

The element density method (forward analysis) : $\mathbf{C}_e = \gamma_e^n \mathbf{C}_0$ (27)

The element density method (sensitivity analysis) : $s\mathbf{C}_e = \gamma_e^{n_s} \mathbf{C}_0$ (28)

where the penalization factors for the forward and sensitivity analyses are n and n_s , respectively.

As previously explained, a main idea of the ECP method is that the constitutive matrix of the discretizing elements remains a constant matrix.

Forward analysis in the ECP method : $s\mathbf{C}_e = \mathbf{C}_0$ (29)

From a microstructure point of view, the ECP method adopts a filled solid microstructure. Because the discretizing elements remain solid and the connectivities among finite elements are defined by the zero-length links, the side effects of the element density method can be resolved. Moreover, we are concerned about still being able to use the constant constitutive matrix for the stable convergence of the original STOM for geometrical nonlinearity. However, in this research, our many numerical tests reveal that the original ECP method cannot overcome the local optima issue and the singularity issue. The stress constraints should not be considered when the associated elements are modeled for the void region, and the no-structure without any solid domain should be removed from the candidates of optimal solutions. Therefore, the present study has determined that the ECP method still needs the following interpolation of the

constitutive matrix with respect to the design variable assigned to the e th finite element:

$$\text{Sensitivity analysis of the ECP method: } \mathbf{C}_e = \gamma_e^{n_{ECP-S}} \mathbf{C}_0 \quad (30)$$

To show that the above constitutive matrix and the penalization factor are used for the sensitivity analysis of the ECP method, the associated penalization factor is denoted by n_{ECP-S} . Then, it becomes an important issue to determine how to choose these penalization factors for stable convergence in the stress-based topology optimization of a geometrically nonlinear structure.

After further analysis, this research determined the following relationship for the penalization factors of the element density-based approach and the ECP method for stable optimization convergence.

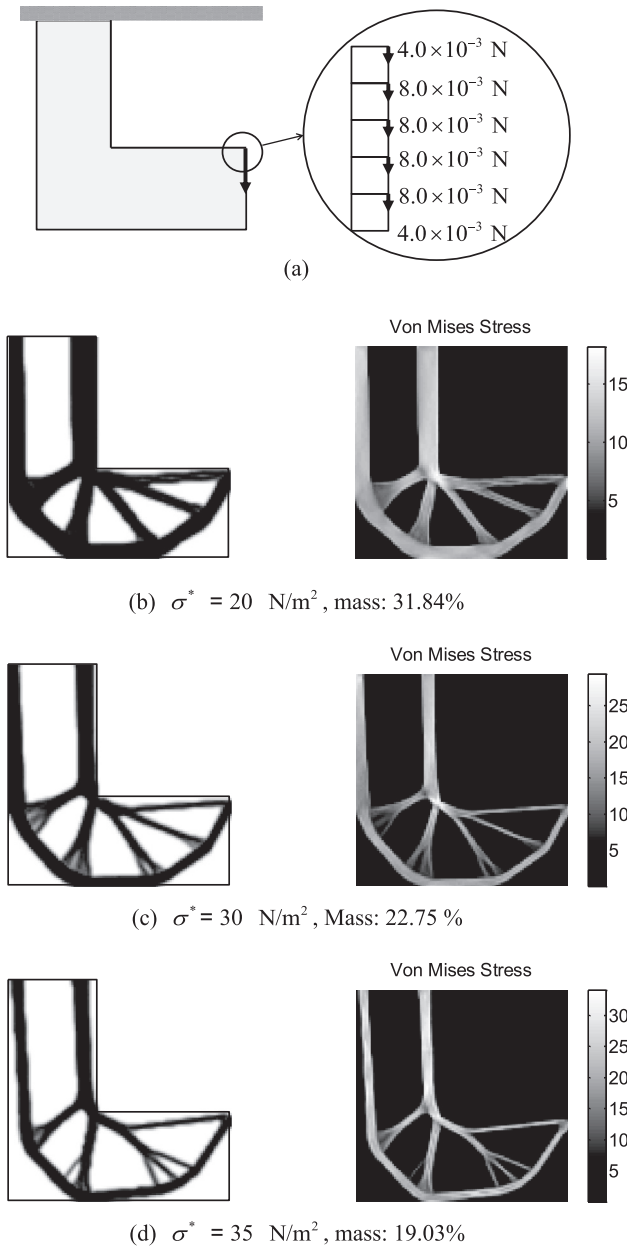


Fig. 8. L-shaped structure and optimization results. (a) A problem definition (loading factor = 40), (b) an optimized design with 31.84% mass usage for the maximum stress limit $\sigma^* = 20 \text{ N/m}^2$, (c) an optimized design with 22.75% mass usage for the maximum stress limit $\sigma^* = 30 \text{ N/m}^2$, and (d) an optimized design with 19.03% mass usage for the maximum stress limit $\sigma^* = 35 \text{ N/m}^2$.

$$\underbrace{n - n_s}_{\text{The element density based approach}} = \underbrace{0 - n_{ECP-S}}_{\text{The ECP method}} \quad (31)$$

The above relationship can be derived by considering that the stress components and corresponding von Mises stress are proportional to the n power of a design variable and approximately inversely proportional to the n_s power of a design variable. In other words, they are approximately proportional to the difference between the penalty values, i.e., $n - n_s$. Because the ECP method has the same characteristics as the element density-based approach, at least for linear structural topology optimization, the ECP method also has the singularity issue and the local optima issue. To cope with these issues, the ECP method similarly requires an appropriate penalty value for the sensitivity analysis to satisfy the above relationship, as expressed in Eq. (31). This relationship also indicates that, when using the penalty values satisfying the above relationship of the element density-based approach, very similar designs can be obtained with the SIMP method. Therefore, any combination with the same constant $n - n_s$ provides similar layouts.

Because the penalty factor of the ECP method, n_{ECP-S} , is set to a negative value, the power of the lower bound, 0, becomes infinity. Therefore, the values of the 2nd PK stress are calculated by using the following rule and introducing the lower bound γ of the design variable, as follows:

$$\mathbf{S} = \max(\gamma, \gamma_e)^{n_{ECP-S}} \mathbf{C}_0 \mathbf{E}, \quad \gamma = 0.01 \quad (32)$$

3.2. Sensitivity analysis

To conduct the STOM using a gradient-based optimizer, the sensitivity values of the local stress constraints should be calculated. The sensitivities of the objective function, volume (as expressed in Eq. (22)) can be easily calculated, whereas the calculation of the sensitivities of the local stress constraints becomes more complicated. By using the chain rule, the sensitivities of the k th p -norm stress can be derived as follows:

$$\begin{aligned} \frac{d\langle \sigma_{PN} \rangle_k}{d\gamma_e} &= \frac{\partial \langle \sigma_{PN} \rangle_k}{\partial \gamma_e} + \frac{\partial \langle \sigma_{PN} \rangle_k}{\partial \sigma_e} \frac{\partial \sigma_e}{\partial \gamma_e} \frac{\partial \sigma_e}{\partial \mathbf{S}_e} \frac{\partial \mathbf{S}_e}{\partial \mathbf{U}} \frac{\partial \mathbf{U}}{\partial \gamma_e} + \sum_{e'=1}^{NE} \frac{\partial \langle \sigma_{PN} \rangle_k}{\partial \sigma_{e'}} \frac{\partial \sigma_{e'}}{\partial \mathbf{S}_{e'}} \frac{\partial \mathbf{S}_{e'}}{\partial \mathbf{U}} \frac{\partial \mathbf{U}}{\partial \gamma_e} \\ &\times \frac{\partial \sigma_{e'}}{\partial \mathbf{S}_{e'}} \frac{\partial \mathbf{S}_{e'}}{\partial \mathbf{U}} \frac{\partial \mathbf{U}}{\partial \gamma_e} \end{aligned} \quad (33)$$

The variable $\sigma_{e'}$ represents the e' stress component. The adjoint variable λ_k^T is introduced for the sensitivity analysis and can be obtained from the derivatives of the static equilibrium equation, as follows:

$$\mathbf{K}_T \lambda_k = - \sum_{e'=1}^{NE} \frac{\partial \langle \sigma_{PN} \rangle_k}{\partial \sigma_{e'}} \left(\frac{\partial \sigma_{e'}}{\partial \mathbf{S}_{e'}} \frac{\partial \mathbf{S}_{e'}}{\partial \mathbf{U}} \frac{\partial \mathbf{U}}{\partial \gamma_e} \right)^T \quad (34)$$

It is assumed that the external force is independent of the density design variables. By plugging Eq. (34) into Eq. (33), the sensitivity value of the p -norm of the von Mises stresses can be derived using the adjoint variable λ_k^T such that

$$\frac{d\langle \sigma_{PN} \rangle_k}{d\gamma_e} = \frac{\partial \langle \sigma_{PN} \rangle_k}{\partial \gamma_e} + \frac{\partial \langle \sigma_{PN} \rangle_k}{\partial \sigma_e} \frac{\partial \sigma_e}{\partial \mathbf{S}_e} \frac{\partial \mathbf{S}_e}{\partial \mathbf{U}} \frac{\partial \mathbf{U}}{\partial \gamma_e} + \lambda_k^T \frac{d\mathbf{K}_T}{d\gamma_e} \mathbf{U} \quad (35)$$

The terms in Eq. (35) are derived as follows:

$$\frac{\partial \langle \sigma_{PN} \rangle_k}{\partial \gamma_e} = \frac{1}{p} \left(\sum_e (\sigma_e^p \gamma_e) \right)^{\frac{1}{p}-1} (\sigma_e^p) \quad (36)$$

$$\frac{\partial \langle \sigma_{PN} \rangle_k}{\partial \sigma_e} = \left(\sum_e \left(\frac{\sigma_e}{\sigma^*} \right)^p \gamma_e \right)^{\frac{1}{p}-1} \gamma_e \left(\frac{\sigma_e}{\sigma^*} \right)^{p-1} \frac{p}{\sigma^*} \quad (37)$$

$$\frac{\partial_0^{t+\Delta t} \mathbf{S}_e}{\partial \gamma_e} = \frac{n_{ECP-s}}{\gamma_e} \mathbf{S}_e \quad (38)$$

$$\frac{\partial_0^{t+\Delta t} \mathbf{S}_e}{\partial_0^{t+\Delta t} \mathbf{U}} = \gamma_e^{n_{ECP-s}} \mathbf{C}_0 \mathbf{B} \quad (39)$$

4. Analysis and topology optimization examples

This section shows the validity of the present formula for the penalty factors in the ECP approach. This is done by analyzing the stress values of some intuitive structures, along with the validity of the present STOM procedure for a geometrically nonlinear structure, through solving the two illustrative layout optimization problems: an L-shaped structure and a cantilever example. As an

optimization algorithm, the method of moving asymptotes is employed [45].

4.1. Analysis examples

4.1.1. Straight bar analysis with geometrical linearity

For the purpose of understanding the importance of the relationships of the involved penalty factors represented in Eqs. (27)–(31), not only for the element density method but also for the ECP method, let us consider a simple straight structure discretized by five 1-by-1 QUAD elements, as shown in Fig. 2. Although many similar studies of the qp -relaxation of a stress constraint in the SIMP approach have previously been performed, we aim to extend the discussion to include the interpolation factors of the ECP method. With the simple tension condition and a boundary value of zero for Poisson's ratio, a constant stress in the x-direction should be obtained, regardless of the values of the design variables assigned by the linear elasticity theory: $stress = force/area$. Using the same penalty factor for both n and n_s , i.e.,

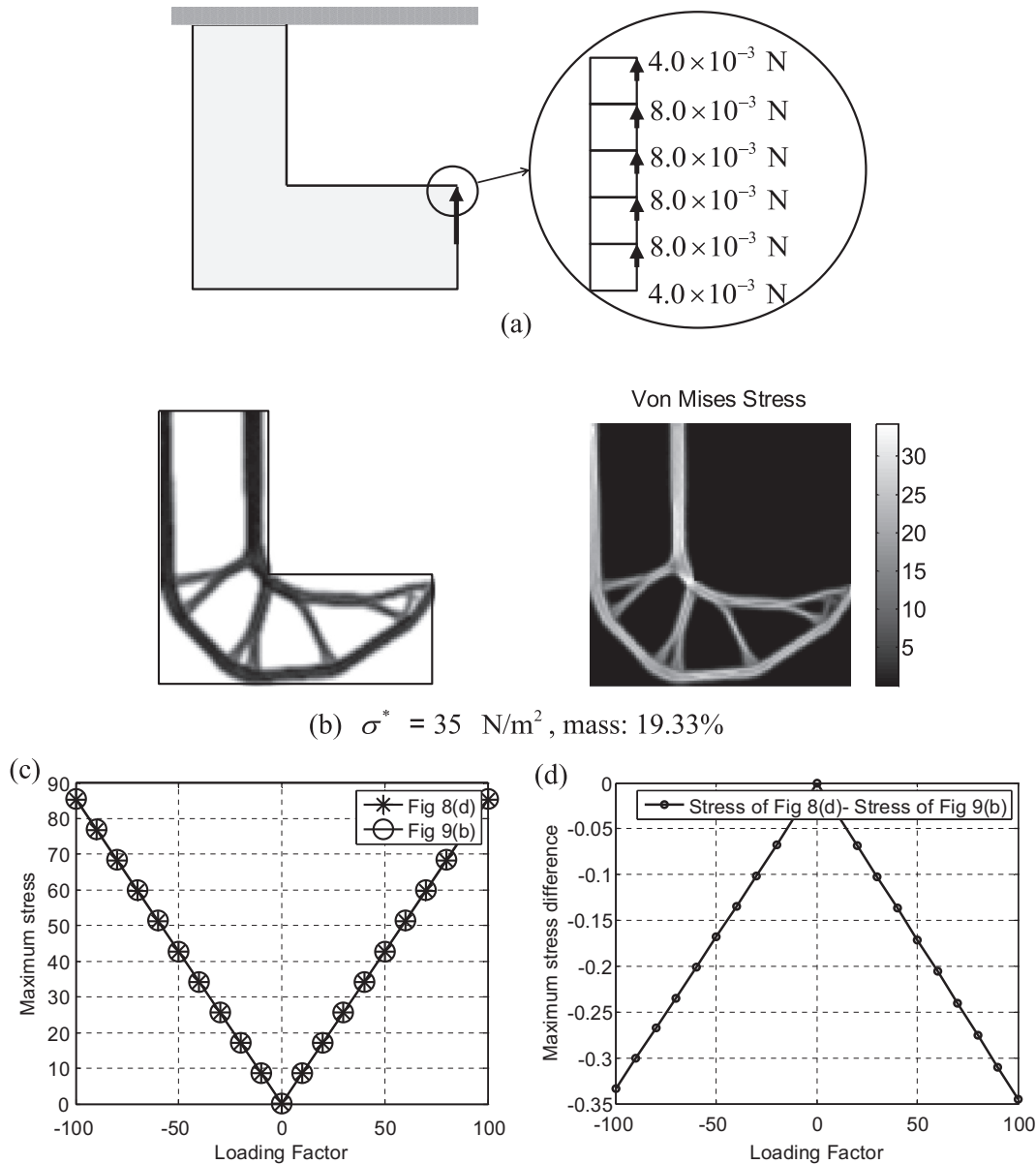


Fig. 9. L-shaped structure and optimization results. (a) A problem definition (loading factor = -40), (b) an optimized design with 19.33% mass usage for the maximum stress limit $\sigma^* = 35$ N/m², and (c) and (d) the maximum stress values (the values are too close to distinguish the stress values of the two designs) and their differences in the two designs.

$n = n_s \in \{\dots -3, -2, -1, 0, 1, 2, 3 \dots\}$, the von Mises stress value σ_{von} evaluated at the center of the left-most finite element becomes one, regardless of the design variables. Because the stress value is not influenced by the values of the design variables or by the penalty factors, even when these have negative integer values, it can be postulated that the strain measure, rather than the stress measure, may be appropriate to use for constraining the deformations of finite elements. From an optimization point of view, the global optimum of the STOM with a stress limit larger than 1 is “no-structure” (null-structure) or a void structure simulated by a weak Young’s modulus in this simple bar case. Therefore, TO with the same penalty factor suffers from an intermediate design variable issue for general boundary conditions. Thus, as inspired by the earlier research [33], which used the stress constraints to improve the conventional compliance based design, it may be necessary to introduce compliance as either an objective function or a constraint(s), to make a stiffer structure as a local optimum. As an alternative, different penalization factors could be employed for the forward analysis and post-processing analysis for stress, i.e., the qp -relaxation method.

The stress values of the straight beam structure are plotted in Fig. 2(b) for some combinations of penalty values with the element density-based approach for the STOM. As shown, with the penalty factors suggested by the related research on the element density-based approach, i.e., 3 for n and 0.5 for n_s , or 3 for n and 2.5 for n_s , the stress value increases as the design variable approaches the lower-bound value. Therefore, an optimization algorithm would minimize the usage of volume, considering the stress limit that we want to achieve, and a non-design structure would not be optimal with these combinations of penalty factors, satisfying the conditions in Eqs. (27)–(31). It is worthwhile to notice in these simple examples that the penalization factors for the stress-based topology optimization in the framework of the element density-based method play an important role in obtaining a physically meaningful design (a globally or locally stiffer structure). In addition, they might not have a role in the convergence of the design variables to either solid or void, as in the compliance minimization problem, which is a pure mathematical manipulation to relax the singularity issue.

To complete the comparisons for the penalization factors, we analyze the same structure using the ECP method. The ECP method inherits the same singularity issue and local optima issue: the constant stress is obtained with “0” for n_{ECP-S} . Thus, to resolve this issue in the ECP method with “0” for the penalty factor of the forward analysis, it is found that the $n - n_s$ value of the SIMP method should be used for $-n_{ECP-S}$. With this special value of n_{ECP-S} satisfying $-n_{ECP-S} = n - n_s$, the exact behavior of the stress value of the SIMP method can be recovered, as shown in Figs. 2(d) and 3. In Fig. 2, tension loads are applied, and in Fig. 3, vertical loads are applied to the same structure with the same boundary conditions. Note that, with the penalty factor of the ECP method satisfying Eq. (31), the exact stress evaluation of the SIMP method can be obtained using the ECP method, as shown in Figs. 2(d) and 3.

4.1.2. Straight bar example with geometrical nonlinearity

To consider the von Mises stress behaviors of the SIMP and ECP methods for a geometrically nonlinear structure, we recalculate the stress values by varying the design variable of a simple extension structure and simple bending structure, as shown in Figs. 4 and 5, using the Kirchhoff material assumption (linear material). For the first simple extension structure shown in Fig. 2, the analytical solution can be obtained as follows:

$$\text{X-direction GL strain : } {}_0^{t+\Delta t}\epsilon_{xx} = {}_0^{t+\Delta t}u_{x,x} + \frac{1}{2} {}_0^{t+\Delta t}u_{x,x}^2 \quad (40)$$

$$\begin{aligned} \text{Equilibrium of SIMP : } & \underbrace{\left(1 + {}_0^{t+\Delta t}u_{x,x}^2\right) \left({}_0^{t+\Delta t}u_{x,x} + \frac{1}{2} {}_0^{t+\Delta t}u_{x,x}^2\right) E_0 \gamma^n A}_{\text{Internal Force}} \\ & = \underbrace{F}_{\text{External Force}} \quad (E_0 = F = A = 1) \end{aligned} \quad (41)$$

$$\text{Stress of SIMP : } \sigma_{von} = \left({}_0^{t+\Delta t}u_{x,x} + \frac{1}{2} {}_0^{t+\Delta t}u_{x,x}^2\right) E_0 \gamma^{n_s} \quad (42)$$

$$\begin{aligned} \text{Equilibrium of ECP : } & \underbrace{\left(1 + {}_0^{t+\Delta t}u_{x,x}^2\right) \left({}_0^{t+\Delta t}u_{x,x} + \frac{1}{2} {}_0^{t+\Delta t}u_{x,x}^2\right) E_0 A}_{\text{Internal Force}} \\ & = \underbrace{F}_{\text{External Force}} \quad (E_0 = F = A = 1) \end{aligned} \quad (43)$$

$$\text{2nd PK stress of ECP : } \sigma_{von} = \left({}_0^{t+\Delta t}u_{x,x} + \frac{1}{2} {}_0^{t+\Delta t}u_{x,x}^2\right) E_0 \gamma^{n_{ECP-S}} \quad (44)$$

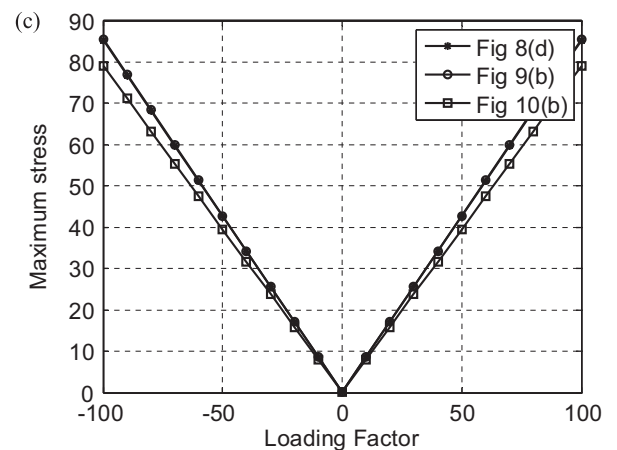
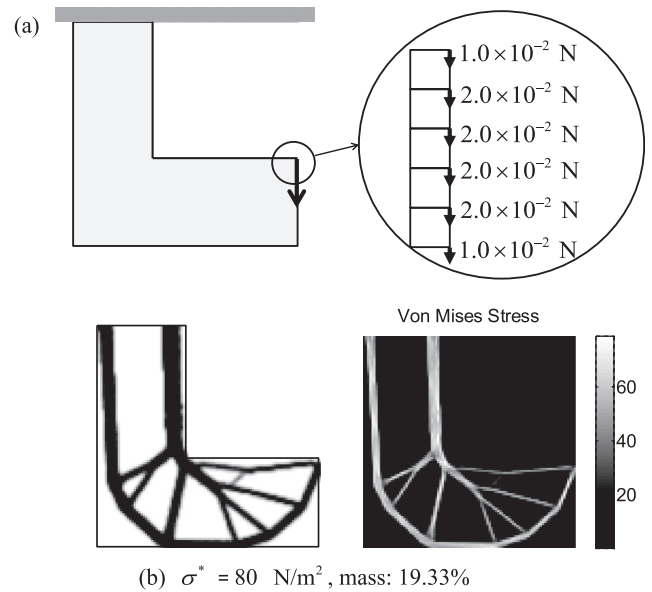


Fig. 10. L-shaped structure and optimization results. (a) A problem definition (loading factor = 100), (b) an optimized design with 19.93% mass usage for the maximum stress limit $\sigma^* = 80 \text{ N/m}^2$, and (c) the stress comparison.

It is important to note that the curves of the von Mises stress, calculated by FE with respect to the *solid* design variables, are compared with the above analytical solutions and plotted in Fig. 4. As shown, the curves of the von Mises stress for this simple extension structure are similar to those for the linear structure. However, in the case of the bending load, because of the buckling of the structure modeled by the SIMP approach, a bumping curve is obtained, as shown in Fig. 5.

4.2. Topology optimization examples

4.2.1. Example 1: L-bracket example

For the first topology optimization example, the well-studied L-shaped structure is considered. The design domain is 0.1 m by 0.1 m and is discretized using QUAD elements of 0.001 m by 0.001 m. To simulate the upper right hole, the corresponding design variables are set to the lower bound. The top line is clamped,

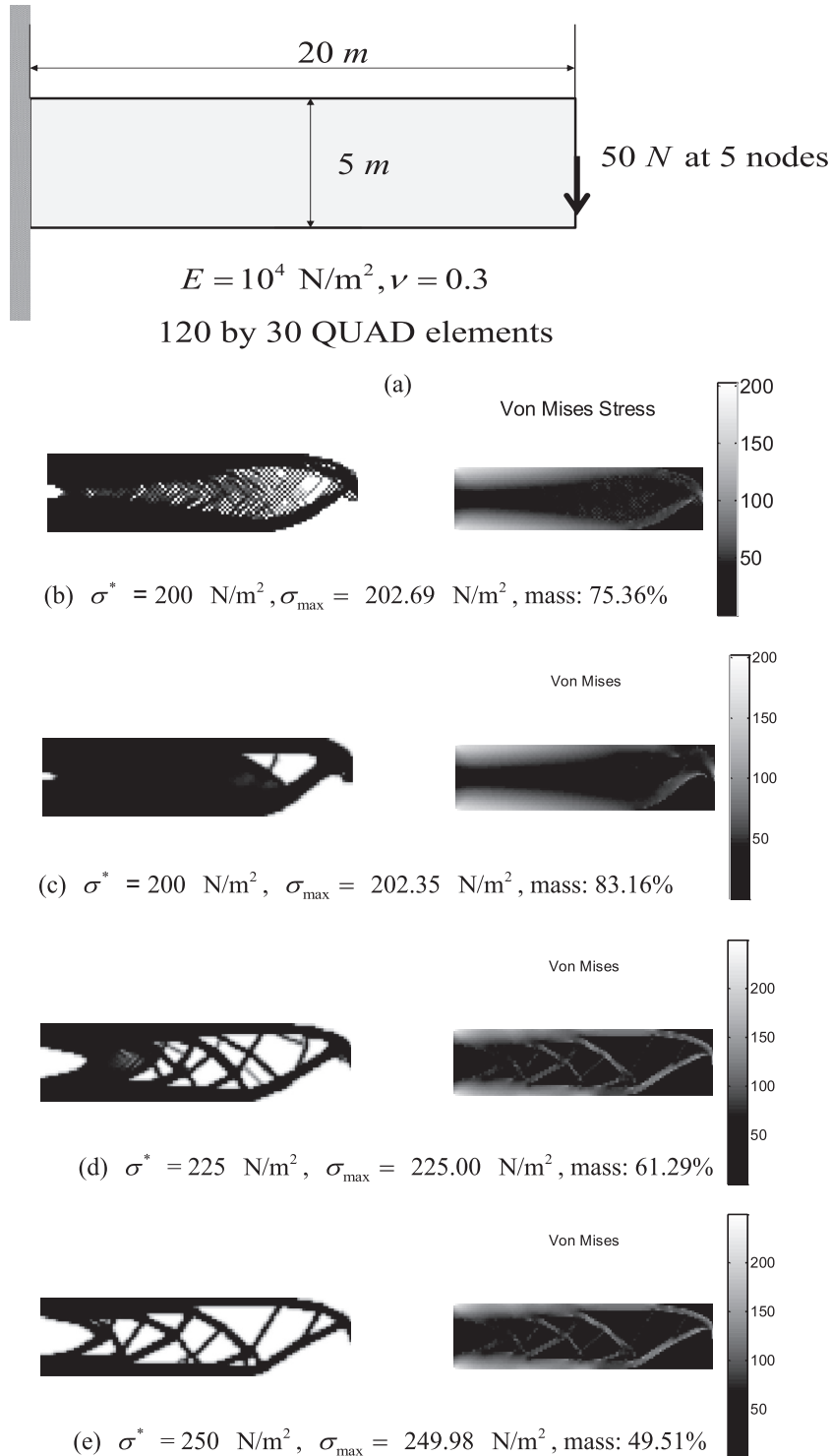


Fig. 11. Sender beam problem. (a) The problem definition, (b) an optimized design with 75.36% mass usage for the maximum stress limit $\sigma^* = 200 \text{ N/m}^2$, (c) an optimized design with 83.16% mass usage for the maximum stress limit $\sigma^* = 200 \text{ N/m}^2$, (d) an optimized design with 61.29% mass usage for the maximum stress limit $\sigma^* = 225 \text{ N/m}^2$, and (e) an optimized design with 49.51% mass usage for the maximum stress limit $\sigma^* = 250 \text{ N/m}^2$.

and a downward structural force of 10^{-3} N is applied at the 5 nodes to remove the stress concentration, as shown in Fig. 6(a). Young's modulus and Poisson's ratio are set to 10^6 N/m² and 0.3, respectively. As previously formulated, we minimize the mass usage, subject to the local von Mises stress of the 2nd PK stress values. Because the magnitude of the applied force is too small, the optimized layouts are similar to those of linear designs, even when considering the geometrical nonlinearity, as shown in Fig. 6. As reported in earlier research, the re-entrant corner is smoothed out and, by decreasing the magnitude of the maximum stress limit, as expected, more mass is used. We also examine the effect of some finite elements and patches of the I-ECP method with intermediate design variables in the results of Fig. 6. To investigate the effects of the intermediate design variables in the stress calculation, hard-kill postprocessing, which sets the design variables over a critical value (i.e., 0.35 here) to ones and the others to zeros, is applied to the designs in Fig. 7. For the design of Fig. 6(a) with $\sigma^* = 0.8$ N/m², the mass ratio of the postprocessed design increases to 24.55%, and its maximum stress value becomes 0.8431 N/m² as a result of the stress concentration at the corner. The number of finite elements whose stress values are greater than σ^* is 2 after the postprocessing. For the design of Fig. 6(b), the mass usage also increases to 22.30%, but the maximum stress value is 0.814 N/m². This example shows that the designs of the stress-based optimization require some shape optimization processes.

To consider geometrical nonlinearity, we magnify the force to 40 times the original force in Fig. 8. By controlling the value of the maximum stress limit, we are able to obtain the optimization results shown in Fig. 8. Here, even though we increased the force, the designs are similar to those obtained using linear analyses, except for the design of Fig. 8(d). Here, note that the magnitudes of the force and the stress limit should be increased together. If we set the same maximum stress limit as in the previous example, even the solid structure cannot satisfy the stress constraints. With too high a stress limit, the optimizer uses less mass, which leads to unstable responses of the intermediate structure, and some degenerated designs with numerous intermediate design variables are obtained as a result of some buckling of the solid part. Furthermore, by investigating the results shown in Fig. 8(d) with higher stress limits, we observe that the right vertical bars of the design become inclined because of the geometrical nonlinearity. Thus, although the structural displacements of the final design are small enough, it is likely that the geometrical nonlinearity plays an important role in intermediate designs. To test this aspect further, the upper direction forces are applied, as shown in Fig. 9, with the same conditions as in Fig. 8(d). As shown, the right bars become straight again, which indicates that the design of Fig. 8(d) is influenced by the geometrical nonlinearity. Moreover, Fig. 9(b) and (c) proves that the designs are optimized for their loading conditions.

By investigating the optimized layouts shown in Figs. 8 and 9, we notice that the geometrical nonlinearity does influence the designs. However, as stated above, the structural displacements for the final designs are in the range of geometrical linearity, with some large displacements for the intermediate designs. One of the reasons is that the geometry and its design domain are too small to have large displacements. Testing the above optimization formulation for forces with scaling factors higher than 40 reveals that, because of the buckling of the intermediate designs, some degenerated layouts with numerous intermediate design variables and compliances that are too high are obtained, even with the present qp -formulation for the ECP method. These trials show the possibility of the presence of several local optima and also show the possible lack of global convergence in the case of singular topologies.

To overcome this phenomenon for singular topologies with high scaling factors, we consider the addition of a compliance constraint

to the optimization formulations, as expressed in Eq. (45), in the next optimization example. Until now, we did not attempt to use a compliance measure as either an objective or a constraint, because having the compliance measure may help an optimizer to easily obtain a globally stiffer structure, and having it may unnecessarily confuse STOM designs with some layouts influenced by the compliance measure. However, by setting the compliance limit to a high value only to prevent buckling, we hope to stabilize the

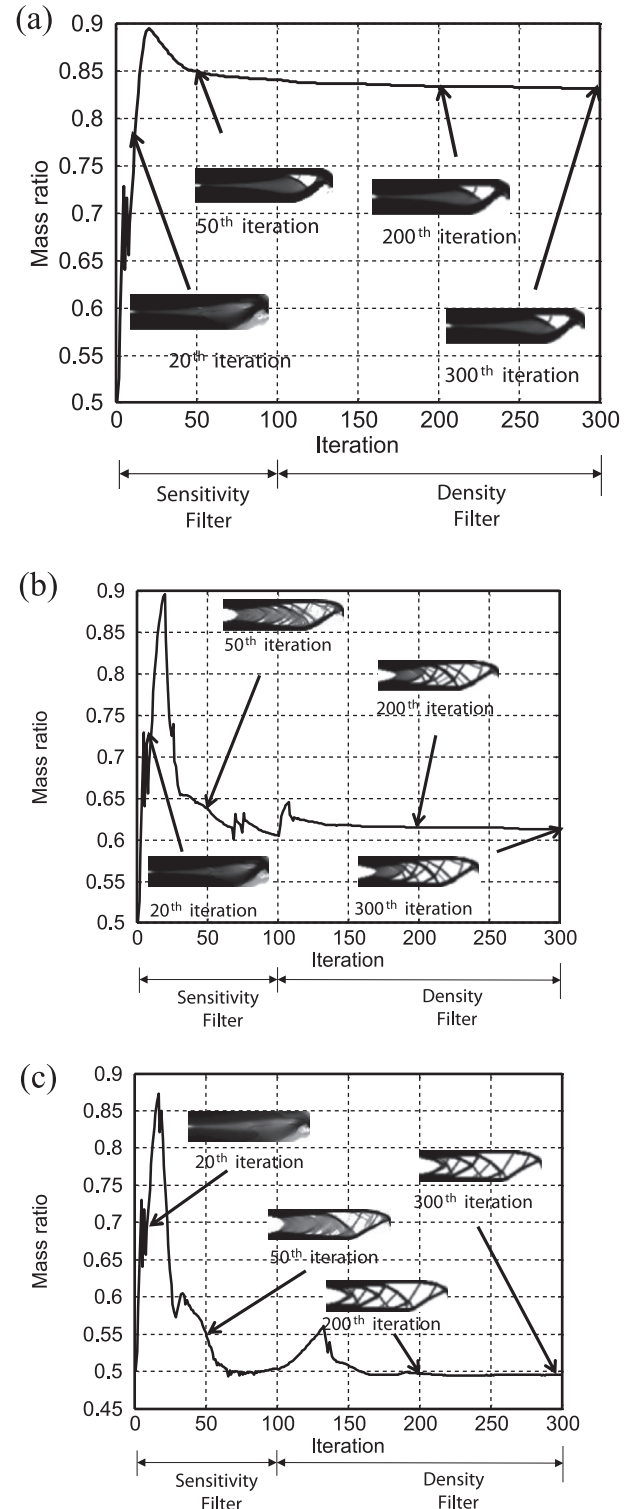


Fig. 12. Optimization history of designs in Fig. 11.

optimization process in the presence of large forces and prevent the degeneration of designs, as shown in Eq. (45). Furthermore, in the present ECP method, if the structural displacements of a structure are too large, the density filtering method that smoothes the design variables (the stiffness values of the zero-length links) before the forward analysis is not suitable in the STOM for a geometrically nonlinear structure. This is because the structural responses before and after the density filtering are too different. Thus, in the next example, we first apply a mesh-independent sensitivity filter to the sensitivity values, and then, after some optimization iterations, we apply the density filter. It is also possible to use the sensitivity filter alone:

$$\begin{aligned}
 & \underset{\gamma}{\text{Minimize}} \quad V(\gamma) = \sum_{e=1}^{NE} \gamma_e v_e \\
 & \text{subject to} \quad \langle \sigma_{\max} \rangle_1 \leq \sigma^* \\
 & \quad \quad \quad \langle \sigma_{\max} \rangle_2 \leq \sigma^* \\
 & \quad \quad \quad \vdots \\
 & \quad \quad \quad \langle \sigma_{\max} \rangle_{RN} \leq \sigma^* \\
 & \text{Compliance} = \mathbf{F}^T \mathbf{U}^* \leq \text{Compliance}^*
 \end{aligned} \tag{45}$$

where the external force and converged displacements are represented by \mathbf{F} and \mathbf{U}^* , respectively.

The allowable compliance limit is Compliance^* , which is chosen here as follows:

$$\text{Compliance}^* = \sum_{i=1}^{NNF} |\text{Maxdisp} \times F_i| \tag{46}$$

where the allowable displacement is Maxdisp , and the non-zero force component is F_i . As shown in Fig. 10, we apply a force 100 times larger than the original force, using a value of 0.025 for Maxdisp (a quarter of the height). Fig. 10(c) shows comparisons of the maximum stress values with respect to the force scaling factor for the three designs shown in Figs. 8(b), 9(b), and 10(b). The maximum stress values with a loading factor of 100 can be seen in Figs. 8(b) and 9(b) to exceed 80 N/m^2 , but with the above formulation, including the additional compliance constraint, it is possible to impose the stress constraint. With a lower loading factor, they show almost similar responses.

4.2.2. Example 2: two-dimensional slender beam structures

For the second numerical example, the long beam structure shown in Fig. 11 is considered. The size of the domain is 20 m by

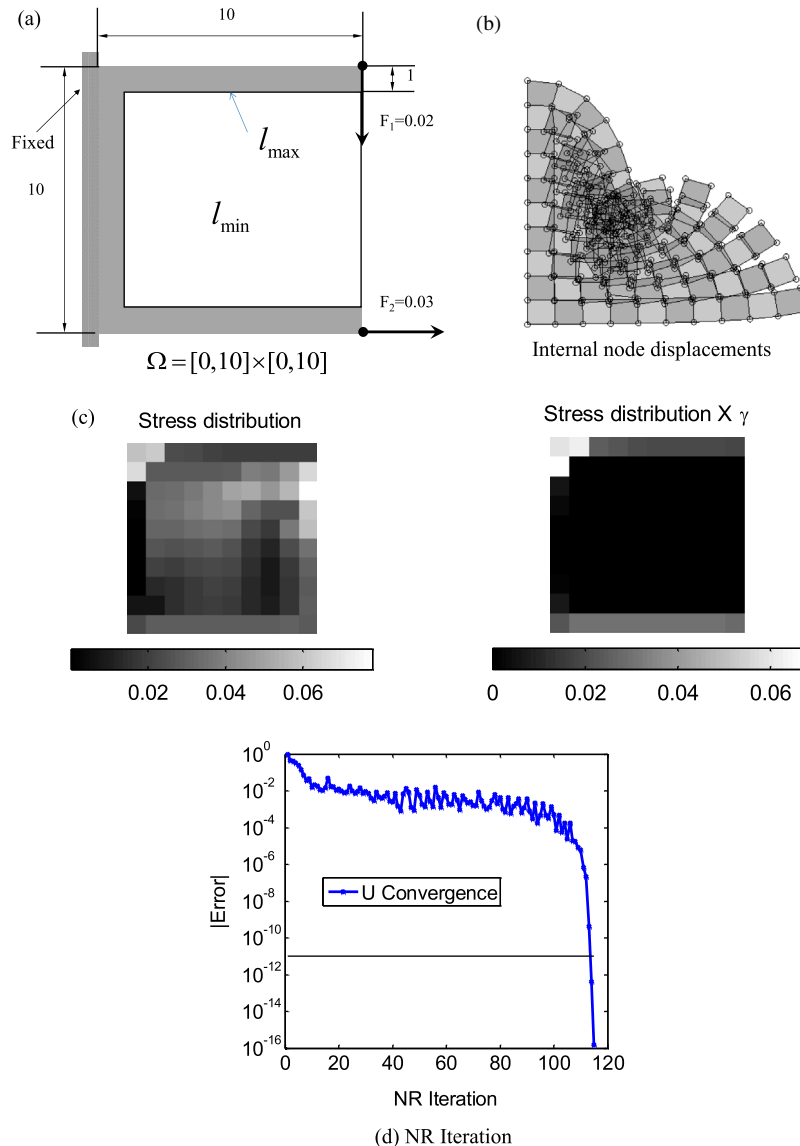


Fig. 13. C bar examples with $(l_{\max} = 10^6, l_{\min} = 10^{-6}, |\Delta \mathbf{U}_{\text{out}}^{(k)}| = \sum_{e=1}^{N_d} (\Delta \mathbf{u}_{e,\text{out}}^{(k)})^2 \leq 10^{-11})$.

5 m, and the domain is discretized with 120-by-30 QUAD finite elements. A downward force of 50 N is applied at the 5 nodes at the right center line to remove the stress concentration. Young's modulus and Poisson's ratio are set to 10^4 N/m² and 0.3, respectively. The number of the region is set to 1.

First, the STOM problem without the density method or the sensitivity filtering method is solved considering the geometrical nonlinearity. The results are presented in Fig. 11(b). Without the geometrical nonlinearity, symmetrical results should be obtained. As expected, there are many checkerboard type patterns, which indirectly indicate that the optimization formulation with the special penalty factors makes a locally or globally stiffer structure constraining their stress values as an optimum. This aspect is also shown in the above analysis in the examples of Figs. 4 and 5. Clearly, the overall layouts look like the tomium of a bird and are very similar to the layouts of the optimum solutions that minimize the compliance subject to the mass constraint. Furthermore, the von Mises stress values are successfully bounded for the prescribed maximum stress limit. Now, the filter is applied to remove the checkerboard pattern for the designs of Fig. 11(c) and (d). As shown, the stress constraints are satisfied, and the designs are similar to the designs obtained by the topology optimization that minimizes the compliance subject to the mass constraint, again without checkerboard patterns [24,28,31]. Furthermore, as previously mentioned, because the density filter significantly changes the density values for the evaluation, it is not efficient for the intermediate designs of this example. Therefore, as shown in Fig. 12, the sensitivity filter is applied to the first 100 iterations, and then a density filter with the same filter radius is applied to obtain the designs. In addition, the sensitivity method can be applied by itself to this problem.

5. Conclusions

This paper developed a stress-based topology optimization method (STOM) for minimizing a volume subject to the local von Mises stress constraints of a geometrically nonlinear structure using the ECP approach. The ECP method is effective at solving the TO of a geometrically nonlinear structure because it parameterizes the link's stiffness values for the connectivity among finite elements, rather than interpolating the material properties of the spatially discretized finite elements. Because of the unstable element issue, in addition to the inherited issues related to the local stress constraints or singularity issue, the highly nonlinear constraint issue, and the existence of too many constraints, investigating the stress constraints of the 2nd PK stress for a geometrically nonlinear structure in TO is an extremely important and difficult research topic. To address this challenge, this paper developed a new STOM optimization process by adopting the ECP method, with which we were able to handle the unstable element issue more efficiently.

However, we found that the singularity issue, the highly nonlinear constraint issue, and the issue of having too many constraints still needed to be solved. In particular, the singularity issue and the local optima issue in the ECP method needed to be properly defined from a design variable parameterization point of view: we needed to determine whether interpolation of the constitutive matrix for the sensitivity analysis is required with respect to the design variables. By comparing Cauchy's and the 2nd PK stress behaviors of some intuitive structures, this paper demonstrated that the ECP method also requires material interpolation with a special penalization factor that satisfies the derived condition, $-n_{ECP-S} = n - n_s$, in the calculation of the stress for locally defined stress constraints. In addition, we observed that, for the STOM

problem, a higher penalization, n , in the SIMP method may not guarantee convergence in the void or solid regions. Rather, the difference between the two penalty factors, $n - n_s$, plays an important role, and the same optimization results can be obtained with the penalty factors in the SIMP method, as long as their differences are the same. It should be emphasized that the forward analysis ($\mathcal{R} = {}^{t+\Delta t}\mathbf{F}_{Ext} - {}^{t+\Delta t}\mathbf{F}_{Int} = \mathbf{0}$) still becomes much more stable in the ECP method, which is essential in the STOM. Moreover, when buckling occurs at solid elements, the ECP method cannot analyze the structure using a standard nonlinear solver. Furthermore, based on the appearance of checkerboard patterns in the results, we conclude that the present stress formulation of the STOM can determine a locally stiffer structure or patterns, but not necessarily a globally stiffer structure. Finally, we were able to obtain some local optima by minimizing a volume subject to the local stress constraints and considering geometrical nonlinearity. With the present approach, it was possible to successfully control the maximum von Mises stress value of the 2nd PK stress value. In future research, we expect that the present approach can be extended to layout designs considering the residual stress constraint with material nonlinearities. Furthermore, the postprocessing issue should be addressed. In this research and some other relevant studies, it is a basic assumption that the stress values at the centers of the discretized finite elements are evaluated and constrained by topology optimization with the relaxed design vari-

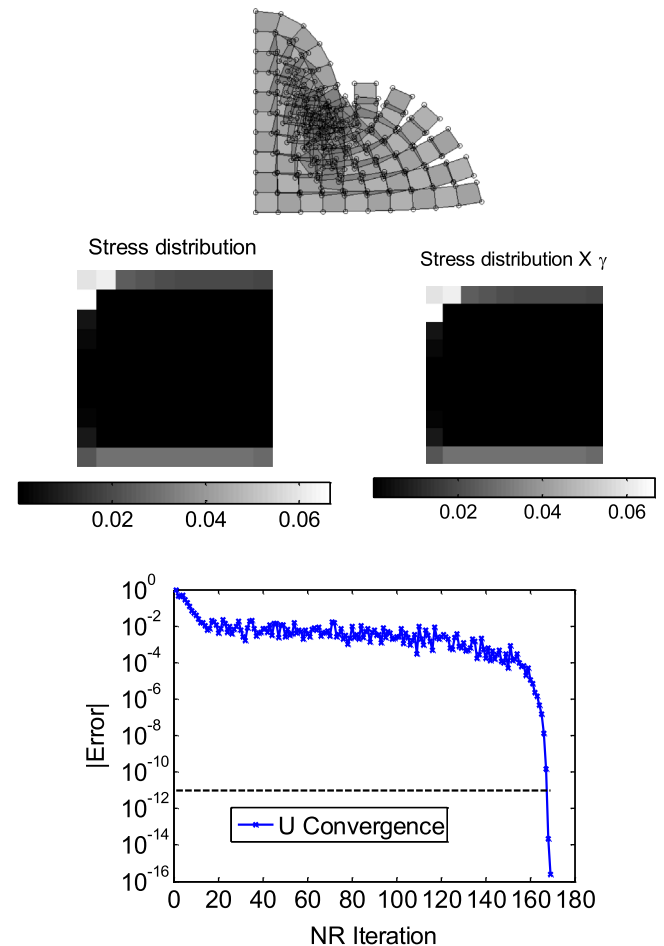


Fig. 14. C bar examples with $(l_{max} = 10^9, l_{min} = 10^{-9}, |\Delta \mathbf{U}_{out}^{(k)}| = \sum_{e=1}^{NP} (\Delta \mathbf{u}_{e,out}^{(k)})^2 \leq 10^{-11})$.

ables, and that the optimized layout by the stress-based topology optimization can be a better initial design for the shape optimization from a stress point of view. To obtain the final design from the

results of the stress-based topology optimization, CAD-based shape optimization can be applied, and some further research is required.

(a) Excessive deformation at the 10th iteration due to the bad condition number

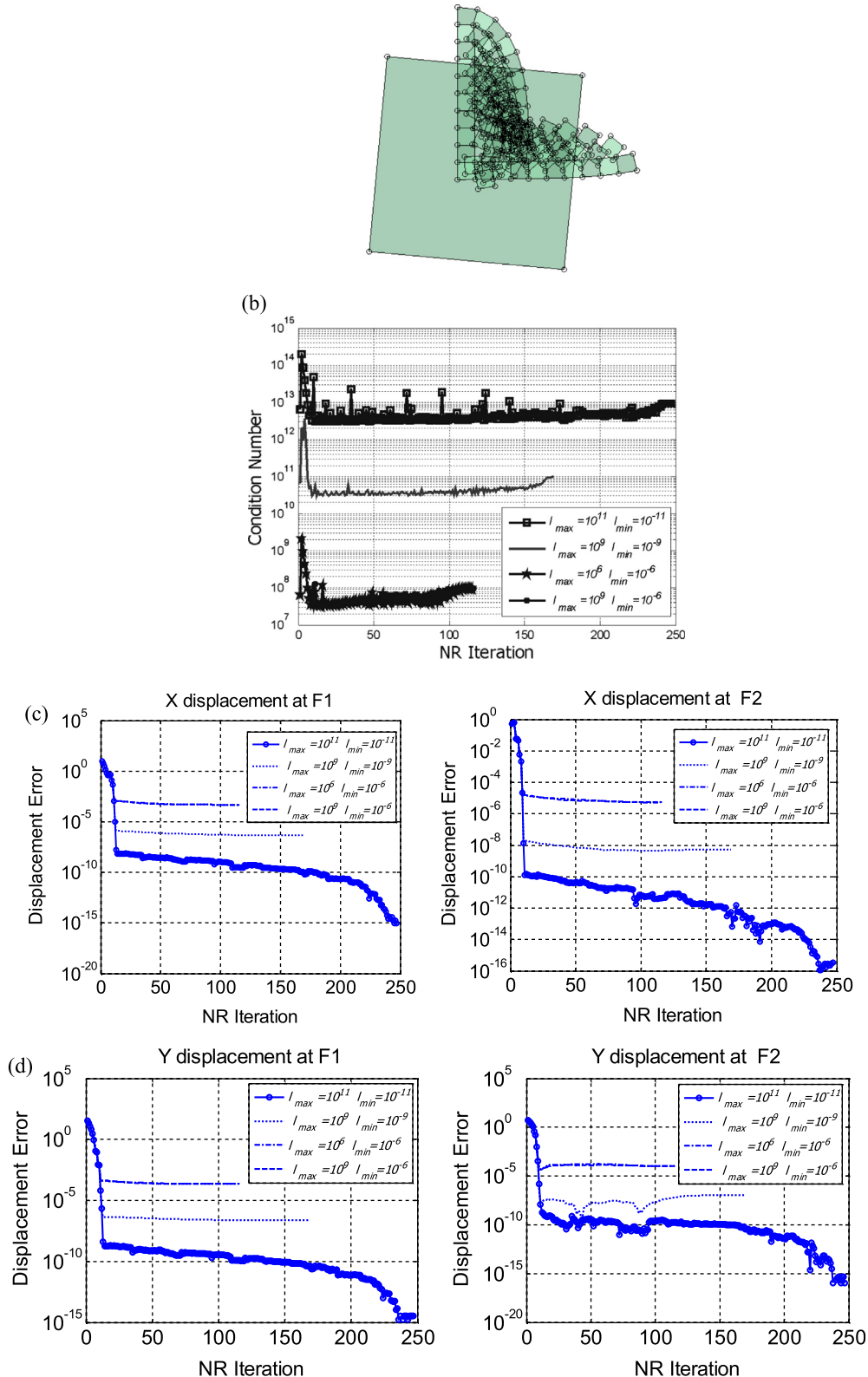


Fig. 15. Some convergence history: (a) excessive deformation due to the band condition number at the 10th iteration and the convergence of the structural displacements, (b) the condition number history, and (c) and (d) the displacement convergence at the nodes with external forces (the displacements of a solid model are set to the reference displacements; the absolute error is calculated).

Acknowledgment

This work was supported by the National Research Foundation of Korea (NRF) grant funded by the Ministry of Education, Science and Technology (NRF- 2012R1A1A2A10038803).

Appendix A.

To consider the convergence with the ECP method, the C structure example is reconsidered in Fig. 13. When this situation is analyzed by the SIMP method, unstable elements inevitably appear at the void region and become troublesome in the NR iteration. However, with the ECP method, because the tangent stiffness remains a positive definite matrix, stable convergence can be obtained. To illustrate the benefits of the internal ECP method over the SIMP method, this structure is analyzed, as shown in Figs. 13 and 14. Because the internal ECP method permits sliding among finite elements without flipping, a stable convergence can be obtained. Note that in the internal ECP method, with too small a stiffness value of the zero-length link, some oscillations are observed in the convergence history due to a bad condition number of the tangent stiffness matrix.

To investigate this oscillation phenomenon in greater detail, the condition number histories with various bounds for l_{\max} , l_{\min} are calculated, as shown in Fig. 15. With $l_{\max} = 10^{11}$, $l_{\min} = 10^{-11}$, some peaks—bad condition numbers—are observed. To investigate this, the deformation at the 10th iteration is plotted in Fig. 15(a). As shown, due to the bad condition number and the snap-through, a large deformation is observed before convergence. Furthermore, it is also observed that the displacement convergence of the solid area is much quicker than that of the void region. To show this, the displacement convergences at the nodes with external forces are plotted in Fig. 15(c) and (d). As shown, the convergence of a design domain varies with respect to the design variables. Thus, from an engineering point of view, it is recommended to use moderated bounds for the link stiffness value.

References

- [1] M.P. Bendsoe, O. Sigmund, *Topology, Optimization: Theory, Methods, and Applications*, Springer, Berlin; New York, 2003.
- [2] T. Borrvall, J. Petersson, Topology optimization of fluids in Stokes flow, *Int. J. Numer. Methods Fluids* 41 (2003) 77–107.
- [3] J.K. Guest, J.H. Prevost, Topology optimization of creeping fluid flows using a Darcy–Stokes finite element, *Int. J. Numer. Methods Engrg.* 66 (2006) 461–484.
- [4] K.H. Sun, S.H. Cho, Y.Y. Kim, Topology design optimization of a magnetostrictive patch for maximizing elastic wave transduction in waveguides, *IEEE Trans. Magn.* 44 (2008) 2373–2380.
- [5] E. Wadbro, M. Berggren, Topology optimization of an acoustic horn, *Comput. Method Appl. Mech.* 196 (2006) 420–436.
- [6] T. Yamamoto, S. Maruyama, S. Nishiwaki, M. Yoshimura, Topology design of multi-material soundproof structures including poroelastic media to minimize sound pressure levels, *Comput. Method Appl. Mech.* 198 (2009) 1439–1455.
- [7] G.H. Yoon, Topology optimization for stationary fluid–structure interaction problems using a new monolithic formulation, *Int. J. Numer. Methods Engrg.* 82 (2010) 591–616.
- [8] G.H. Yoon, J.S. Jensen, O. Sigmund, Topology optimization of acoustic–structure interaction problems using a mixed finite element formulation, *Int. J. Numer. Methods Engrg.* 70 (2007) 1049–1075.
- [9] G.H. Yoon, O. Sigmund, A monolithic approach for topology optimization of electrostatically actuated devices, *Comput. Method Appl. Mech.* 197 (2008) 4062–4075.
- [10] M. Bruggi, On an alternative approach to stress constraints relaxation in topology optimization, *Struct. Multidiscip. Optim.* 36 (2008) 125–141.
- [11] M. Bruggi, P. Venini, A mixed FEM approach to stress-constrained topology optimization, *Int. J. Numer. Methods Engrg.* 73 (2008) 1693–1714.
- [12] G.D. Cheng, X. Guo, Epsilon-relaxed approach in structural topology optimization, *Struct. Optim.* 13 (1997) 258–266.
- [13] P. Duysinx, M.P. Bendsoe, Topology optimization of continuum structures with local stress constraints, *Int. J. Numer. Methods Engrg.* 43 (1998) 1453–1478.
- [14] S.H. Jeong, S.H. Park, D.H. Choi, G.H. Yoon, Topology optimization considering static failure theories for ductile and brittle materials, *Comput. Struct.* 110–111 (2012) 116–132.
- [15] C. Le, J. Norato, T. Bruns, C. Ha, D. Tortorelli, Stress-based topology optimization for continua, *Struct. Multidiscip. Optim.* 41 (2010) 605–620.
- [16] Y.J. Luo, Z. Kang, Topology optimization of continuum structures with Drucker–Prager yield stress constraints, *Comput. Struct.* 90–91 (2012) 65–75.
- [17] J. Paris, F. Navarrina, I. Colominas, M. Casteleiro, Block aggregation of stress constraints in topology optimization of structures, *Adv. Engrg. Softw.* 41 (2010) 433–441.
- [18] G.Y. Qiu, X.S. Li, A note on the derivation of global stress constraints, *Struct. Multidiscip. Optim.* 40 (2010) 625–628.
- [19] G.I.N. Rozvany, Difficulties in truss topology optimization with stress, local buckling and system stability constraints, *Struct. Optim.* 11 (1996) 213–217.
- [20] R.J. Yang, C.J. Chen, Stress-based topology optimization, *Struct. Optim.* 12 (1996) 98–105.
- [21] M. Zhou, Difficulties in truss topology optimization with stress and local buckling constraints, *Struct. Optim.* 11 (1996) 134–136.
- [22] M. Burger, R. Stainko, Phase-field relaxation of topology optimization with local stress constraints, *SIAM J. Control Optim.* 45 (2006) 1447–1466.
- [23] J. Paris, F. Navarrina, I. Colominas, M. Casteleiro, Topology optimization of continuum structures with local and global stress constraints, *Struct. Multidiscip. Optim.* 39 (2009) 419–437.
- [24] T.E. Bruns, O. Sigmund, D.A. Tortorelli, Numerical methods for the topology optimization of structures that exhibit snap-through, *Int. J. Numer. Methods Engrg.* 55 (2002) 1215–1237.
- [25] T.E. Bruns, D.A. Tortorelli, An element removal and reintroduction strategy for the topology optimization of structures and compliant mechanisms, *Int. J. Numer. Methods Engrg.* 57 (2003) 1413–1430.
- [26] S. Cho, H.S. Jung, Design sensitivity analysis and topology optimization of displacement-loaded non-linear structures, *Comput. Method Appl. Mech.* 192 (2003) 2539–2553.
- [27] M. Langelaar, G.H. Yoon, Y.Y. Kim, F. van Keulen, Topology optimization of planar shape memory alloy thermal actuators using element connectivity parameterization, *Int. J. Numer. Methods Engrg.* 88 (2011) 817–840.
- [28] G.H. Yoon, Y.Y. Kim, Element connectivity parameterization for topology optimization of geometrically nonlinear structures, *Int. J. Solids Struct.* 42 (2005) 1983–2009.
- [29] G.H. Yoon, Maximizing the fundamental eigenfrequency of geometrically nonlinear structures by topology optimization based on element connectivity parameterization, *Comput. Struct.* 88 (2010) 120–133.
- [30] G.H. Yoon, Y.Y. Kim, M. Langelaar, F. van Keulen, Theoretical aspects of the internal element connectivity parameterization approach for topology optimization, *Int. J. Numer. Methods Engrg.* 76 (2008) 775–797.
- [31] T. Buhl, C.B.W. Pedersen, O. Sigmund, Stiffness design of geometrically nonlinear structures using topology optimization, *Struct. Multidiscip. Optim.* 19 (2000) 93–104.
- [32] G.H. Yoon, Y.S. Joun, Y.Y. Kim, Optimal layout design of three-dimensional geometrically non-linear structures using the element connectivity parameterization method, *Int. J. Numer. Methods Engrg.* 69 (2007) 1278–1304.
- [33] M. Bruggi, P. Duysinx, Topology optimization for minimum weight with compliance and stress constraints, *Struct. Multidiscip. Optim.* 46 (2012) 369–384.
- [34] M. Stolpe, K. Svanberg, On the trajectories of the epsilon-relaxation approach for stress-constrained truss topology optimization, *Struct. Multidiscip. Optim.* 21 (2001) 140–151.
- [35] Q. Xia, T.L. Shi, S.Y. Liu, M.Y. Wang, A level set solution to the stress-based structural shape and topology optimization, *Comput. Struct.* 90–91 (2012) 55–64.
- [36] X. Guo, G. Cheng, K. Yamazaki, A new approach for the solution of singular optima in truss topology optimization with stress and local buckling constraints, *Struct. Multidiscip. Optim.* 22 (2001) 364–372.
- [37] K.J. Bathe, *Finite Element Procedures*, Prentice-Hall, New Jersey, 1996.
- [38] R.d. Borst, M.A. Crisfield, *Nonlinear Finite Element Analysis of Solids and Structures*, second ed., Wiley, Hoboken, NJ, 2012.
- [39] R.D. Cook, *Concepts and Applications of Finite Element Analysis*, fourth ed., Wiley, New York, NY, 2001.
- [40] J.K. Guest, J.H. Prevost, T. Belytschko, Achieving minimum length scale in topology optimization using nodal design variables and projection functions, *Int. J. Numer. Methods Engrg.* 61 (2004) 238–254.
- [41] O. Sigmund, Morphology-based black and white filters for topology optimization, *Struct. Multidiscip. Optim.* 33 (2007) 401–424.
- [42] G.H. Yoon, S. Heo, Y.Y. Kim, Minimum thickness control at various levels for topology optimization using the wavelet method, *Int. J. Solids Struct.* 42 (2005) 5945–5970.
- [43] G.H. Yoon, Y.Y. Kim, Triangular checkerboard control using a wavelet-based method in topology optimization, *Int. J. Numer. Methods Engrg.* 63 (2005) 103–121.
- [44] G.H. Yoon, Y.Y. Kim, M.P. Bendsoe, O. Sigmund, Hinge-free topology optimization with embedded translation-invariant differentiable wavelet shrinkage, *Struct. Multidiscip. Optim.* 27 (2004) 139–150.
- [45] K. Svanberg, The method of moving asymptotes – a new method for structural optimization, *Int. J. Numer. Methods Engrg.* 24 (1987) 359–373.